PCCP

Accepted Manuscript

This is an *Accepted Manuscript*, which has been through the Royal Society of Chemistry peer review process and has been accepted for publication.

Accepted Manuscripts are published online shortly after acceptance, before technical editing, formatting and proof reading. Using this free service, authors can make their results available to the community, in citable form, before we publish the edited article. We will replace this *Accepted Manuscript* with the edited and formatted *Advance Article* as soon as it is available.

You can find more information about *Accepted Manuscripts* in the **Information for Authors**.

ROYAL SOCIETY OF CHEMISTRY

www.rsc.org/pccp

Probing $\pi \rightarrow \pi^*$ photoisomerization mechanism of cis-azobenzene by multi-state ab initio on-the-fly trajectory dynamics simulation[*]

Le Yu[a,c], Chao Xu[a,b] and Chaoyuan Zhu[a*],

Based on a newly developed algorithm to compute global nonadiabatic switching probability only using electronic adiabatic potential energy surfaces and its gradients, we could be able to perform on-the-fly trajectory surface hopping simulation at the 5SA-CASSCF(6,6)/6-31G quantum level to probe $\pi\pi^*$ photoisomerization mechanism of the azobenzene within four singlet low-lying electronic states (S_0, S_1, S_2, and S_3) coupled with complicated conical intersection network. We found that four conical intersections between the S_1 and S_2 states (one is near cis-isomer region, another near trans-isomer region, and two others in between cis and trans) play the most important role for understanding photoisomerization mechanism of azobenzene upon S_2 and S_3 $\pi\pi^*$ excitation. We classified six cases to demonstrate detailed photoisomerization mechanism by choosing 8 (6) typical reactive (nonreactive) trajectories, namely two-step fast-fast processes having the lifetime from several tenths to hundred femtoseconds and two-step fast-slow and slow-slow processes having lifetime from the several hundreds to thousand femtoseconds. We found for the first time from simulation that once

[a] *Institute of Molecular Science, Department of Applied Chemistry, and Center for Interdisciplinary Molecular Science, National Chiao-Tung University, Hsinchu 300, Taiwan. Email:cyzhu@mail.nctu.edu.tw*

[b] *Department of Chemistry, Beijing Normal University, Beijing 100875, PR China*

[c] *College of Chemistry & Material Science, Northwest University, Xi'an, 710127, P. R. China.*

2

trajectory visits the conical intersection near trans-isomer after $\pi\pi^*$ excitation, it could rapidly go through inversion pathway to trans-azobenzene and this confirms the most recent experimental observation. We performed 536 sampling trajectories (336 from S_2 and 200 from S_3) initially starting from Franck-Condon region of cis-azobenzene, we obtained total reactive quantum yield 0.3~0.45 in very good agreement with the recent experiment results 0.24~0.50. Moreover, the present method can estimate overall nonadiabatic transition probability for each sampling trajectory from the beginning to the end. This can greatly speed up convergence of nonadiabatic molecular dynamic simulation and for instance it results in quantum yield 0.53 estimated just from 8 typical reactive trajectories.

1. Introduction

The photo-response properties from the trans-to-cis and cis-to-trans isomerizations of azo-group within azobenzene and its derivatives have attracted great attention in molecular photoswitches[1] with a variety of applications in high-density information storage devices,[2,3] light-driven molecular motors,[4,5] and protein probes.[6,7] The photoisomerization mechanism of azobenzene has been roughly classified as four types, namely rotation (torsion of CNNC moiety), inversion (simultaneous inversion motion of both NNC angles), inversion-assisted rotation (pedal-like concerted motion of phenyl rings and nitrogen atoms) and concerted inversion (via linear transition state with both NNC angles increase to 180° simultaneously). The abundant experimental and theoretical investigations reported in the literature enhance our understanding about azobenzene photoisomerization, such as rotation dominated processes, several low-lying singlet-excited states involved conical intersection network, and UV-VIS irradiation wavelength dependence of quantum yield. There is excellent review article[8] which presents achievements and remaining challenges in the subject of azobenzene photoisomerization. On the other hand, theoretical investigations mainly focus on photoisomerization dynamics between electronic ground (S_0) and the first-excited (S_1) states. Lack of molecular dynamical simulation involving in higher excited states makes detailed mechanisms of photoisomerization observed in experiments not satisfactorily explained in theory.

There are a quite few trajectory-based nonadiabatic molecular simulations[9-14] taking into account conical intersection (CI) in the middle of the rotation pathway between S_1 and S_0 states and it corresponds on the $n\rightarrow\pi^*$ excitation. With increasing of both NNC angles via inversion motion, another planar S_1/S_0 CI appears in the inversion pathway near trans-

azobenzene in high energy region.[9] Photoisomerization in inversion pathway is not shown up in simulations since the inversion CI is not energetically accessible upon $n{\rightarrow}\pi^*$ excitation. Therefore, the rotation dominated photoisomerization mechanism on S_1 state is well accepted in theory.

The photoisomerization process upon $\pi{\rightarrow}\pi^*$ excitation is more complicated than the $n{\rightarrow}\pi^*$ excitation case since it is involved contribution from higher electronic excited states. With advances of transient absorption spectroscopic technique, the azobenzene $\pi\pi^*$ band photoisomerization has been becoming a hot topic of subject in experiment. Lednev et al.[15] have performed transient studies on trans-azobenzene and proposed a triple-step decay mechanism in sequential of rotational population in S_2 state, internal conversion of $S_2{\rightarrow}S_1$, and formation of "bottleneck" intermediate component in S_1, and conversion of $S_1{\rightarrow}S_0$ and re-form in the ground state. This model has been confirmed by the other transient experiments with more precisely time constant,[17-23] and similar sequential conversion mechanism for cis-azobenzene after $\pi{\rightarrow}\pi^*$ excitation has been proposed by Satzger et al.[21,22] with much fast time constants. According to the experiment observations, the isomerization process occurs mostly in S_1 state after the fast decay from S_2 via rotation pathway, and then conversion to S_0 state via inversion pathway. Fujino et al.[19,20] have proposed an additional $S_2{\rightarrow}S_1$ fast decay pathway in planar structure for trans-azobenzene with unity quantum yields and this mechanism has been confirmed by Schultz et al.[23] But for the either S_3 or S_4 state in $\pi\pi^*$ excitation band, they have suggested a different uncharacterized relaxation pathway to explain a reduced quantum yield. In the most recent experiment done by Quick et al.,[24] the planar structure $S_n{\rightarrow}S_1$ relaxation ratio of trans-azobenzene has been corrected to be 50%, and the rest S_n population is classified to convert

5

to S_0 state followed by a cascade $S_n \rightarrow S_1 \rightarrow S_0$ relaxation with solely trans product. In this way, quantum yields drop from 0.2 to 0.1 compared with result from $n\pi^*$ excitation. Moreover, for cis-azobenzene upon $\pi\pi^*$ excitation, they proposed that about 30% of the excited species experience fast S_n/S_1 decay and isomerize to trans form in S_1 on a 0.1 ps time scale.

Based on experimental results mentioned above, it is quite demanding on trajectory-based nonadiabatic molecular dynamics simulation that should be able to provide detailed mechanisms of photoisomerization involving in highly excited states. Actually, in the hybrid theoretical and experimental investigation performed by Schultz *et al.*,[23] the direct ab initio molecular dynamics with complete active space self-consistent field (CASSCF) method has been utilized to demonstrate the initial stage dynamics of trans-azobenzene after $\pi\pi^*$ excitation. There is no evidence for the fast decay $S_2 \rightarrow S_1$ (<50 fs) in planar geometry involved with torsion or inversion pathway, while in S_1 state the fast internal conversion(~50 fs) to S_0 state is found to follow inversion pathway. Sauer *et al.*[25] and Dou and coworkers,[26,27] have performed semiclassical electron-radiation-ion dynamics (SERID) simulations with time-dependent density functional methods, and found unusual results in which the torsion mechanism dominates the isomerization processes for both cis- and trans-azobenzene followed by $\pi \rightarrow \pi^*$ excitation. Persico and coworkers[13, 28, 29] have carried out a massively trajectory surface hopping simulations based on the semiempirical floating occupation molecular orbital configuration interaction (FOMO-CI) methods with or without OPLS force fields for cis- and trans-azobenzene photoisomerization followed by both $n\pi^*$ and $\pi\pi^*$ excitation, and they found that both the trans→cis and cis→trans photoreactions are induced by the torsion pathway of the N=N bond combined with

torsion of the N−C bonds.

There still exist contradictions between experimental and theoretical analysis about mechanism of azobenzene photoisomerization for the specific process followed by $\pi\pi^*$ excitation. The theoretical difficulty in conventional trajectory-based surface hopping methods arises from ab initio calculation of nonadiabatic coupling vector involved in multiple coupled-electronic-excited states, and this calculation is very time-consuming that prevents feasible trajectory propagation in numerical simulation. Fortunately, we have newly developed the method to compute nonadiabatic switching probability without calculating nonadiabatic coupling vector.[9] In the present trajectory-based surface hopping method, we need only compute energies of two adjacent adiabatic potential energy surfaces and its gradients among multiple coupled-electronic-excited states. Basically, computation cost for two or more than two electronic states is the almost same. The present method provides a powerful tool to simulate the photoisomerization step by step upon $\pi\pi^*$ excitation and can explain the recent experimental observation. The azobenzene photoisomerization undergoes very complicated isomerization pathways through complicated conical intersection network, besides cis-to-trans and trans-to-cis are quite different. We would take into account cis-to-trans in the present report and put trans-to-cis in the other publication. The present trajectory-based surface hopping method can probe mechanism of azobenzene photoisomerization in great details and provide clear picture about how trajectory travels from beginning, approaching which conical intersection in intermediate process, and reaching to end among four coupled low-lying electronic states (S_0, S_1, S_2, and S_3).

In section 2, we first give a brief description of the present trajectory-based surface

hopping method and how ab initio quantum chemistry method CASSCF is incorporated

into the present nonadiabatic molecular dynamic simulation on on-the-fly potential energy

surfaces. In section 3, we show a detailed understanding of the cis-azobenzene

photoisomerization and discuss mainly on S_2 and S_3 excited states upon the $\pi\pi^*$ excitation

from six distinct isomerization schemes. The results obtained here provide a good

explanation for the different isomerization mechanisms observed in the recent experiment.

2. Theoretical methods and computation details

We calculate on-the-fly trajectory on the potential energy surfaces based on ab initio CASSCF

method by numerically integrating the Newtonian equation of motion with the velocity-Verlet

method.[30] Along trajectory propagation, we detect avoided crossing point by computing

minimum separation between two adjacent adiabatic potential energy surfaces within three

consecutive time steps (this usually is in conical intersection zone). At this avoided crossing,

we compute global nonadiabatic switching probability according to the improved Landau-

Zener formula by Zhu and Nakamura,[31,32]

$$p = \exp\left[-\frac{\pi}{4\sqrt{a^2}}\sqrt{\frac{2}{b^2 + \sqrt{|b^4 \pm 1|}}}\right], \tag{1}$$

in which two unitless parameters, namely effective coupling and effective collision energy, are

given by

$$a^2 = \frac{\hbar^2}{2\mu}\frac{\sqrt{|F_2 F_1|}|F_2 - F_1|}{(2V_{12})^3} \tag{2}$$

and

$$b^2 = \left(E_t - E_X\right)\frac{\left|F_2 - F_1\right|}{\sqrt{\left|F_2 F_1\right|}\left(2V_{12}\right)} \tag{3}$$

in which F_1 and F_2 are forces on two diabatic potential energy surfaces, V_{12} is diabatic coupling,

μ is reduced mass of diatomic molecule, E_X is energy at crossing point and E_t is potential

energy plus kinetic energy component in direction of hopping vector (note + (-) in eqn (1)

stands for $F_1 F_2 > 0$ ($F_1 F_2 < 0$)). Diabatic coupling V_{12} in eqn (2) is directly computed by energy

separation between two adiabatic potential energy surfaces at avoided crossing. At this avoided

crossing, we convert mass-scaled multidimensional forces into mass-scaled one-dimensional

forces given in eqn (2) and eqn (3),[9]

$$\frac{\left|F_2 - F_1\right|}{\sqrt{\mu}} = \sqrt{\sum_{i=1}^{N}\frac{1}{m_i}\sum_{\alpha=x,y,z}\left(F_2^{i\alpha} - F_1^{i\alpha}\right)^2} \quad, \tag{4}$$

and

$$\frac{\sqrt{\left|F_2 F_1\right|}}{\sqrt{\mu}} = \sqrt{\left|\sum_{i=1}^{N}\frac{1}{m_i}\sum_{\alpha=x,y,z}F_2^{i\alpha}F_1^{i\alpha}\right|} \tag{5}$$

where N is number of nuclei in molecule with the mass m_i ($i=1,2,\ldots,N$), α stands for x, y, and z

component of Cartesian coordinates for the i-th nucleus, and multidimensional diabatic

forces $F_1^{i\alpha}$ and $F_2^{i\alpha}$ are generalized from adiabatic forces within three consecutive time steps

around detected avoided crossing along trajectory. Detailed description along with definition of

hopping direction and momentum change at an attempted trajectory hopping position is given

in the Ref.9. We have defined the present nonadiabatic switching probability as global

switching in contrast to Tully's fewest nonadiabatic switching probability as local switching.

We have developed our own code to perform the present on-the-fly nonadiabatic molecular

dynamics simulation on the azobenzene photoisomerization.

Along an on-the-fly running trajectory, we first determine the minimum potential energy gap regarded as an avoided crossing at which we compute the effective coupling parameter a^2 and the effective collision energy b^2 in eqn (2) and eqn (3). If a^2 is large (say at $a^2 \geq 1000$, switching probability is unit), it means that trajectory switches in diabatic limit in the configuration space very close to geometry of conical intersection, while a^2 is small (say at $a^2 \leq 0.001$, switching probability is zero), it means that trajectory switches in adiabatic limit in the configuration space very far from geometry of conical intersection. We do preliminary on-the-fly nonadiabatic trajectory simulation to find out relation between the minimum energy separation ΔE and effective coupling parameter a^2, and then we can set up energy gap limit beyond which adiabatic switching probability is zero. For the present azobenzene molecule, we set up energy gap $|\Delta E| = 0.3\text{eV}$, and thus any sampling trajectory stays on the current adiabatic potential energy surface if energy gap $|\Delta E|$ between two adjacent adiabatic potential energy surfaces is larger than 0.3eV along the trajectory. Roughly, we can say that $100 > a^2 > 0.01$ is meaningful region contributing nonadiabatic dynamics significantly. In the meanwhile, if b^2 is large (say 100), it means that trajectory has an effective kinetic energy (component of momentum vector projecting on the hopping direction) much larger than potential energy at avoided crossing, while b^2 is small (say 0.1), it means that trajectory has an effective kinetic energy almost equal to potential energy at avoided crossing. Value of $a^2 b^2$ is an absolute number to determine nonadiabatic switching probability in eqn (1).

In our previous work,[9] we have employed trajectory-based on-the-fly surface hopping method to study azobenzene photoisomerization (both cis-to-trans and trans-to-cis) based on only ground and first excited states incorporating with two-state averaged CASSCF method (2SA-CASSCF). Based on consideration of both the accuracy and efficiency for 2SA-CASSCF

method, we have selected six active electrons and six active orbitals, namely CASSCF(6, 6), for performing electronic structure calculation. In our previous paper,[9] the both 6-31G and including polarization function 6-31G* basis sets were carefully compared for vertical excitation energies at cis- and trans-isomers, and there is not much difference for these two basis sets. However, the computational time is doubled by using 6-31G* and thus we finally selected 6-31G. In the present work, we extend dynamic simulation to four singlet low-lying electronic states including the $\pi\pi^*$ excitation, so that five-state average is necessary to be chosen in CASSCF method. Finally, the 5SA-CASSCF(6,6)/6-31G is utilized throughout the present paper for geometry optimization as well as on-the-fly potential energy surfaces with use of computational program of Molpro 2009.1 package.[33] Besides, as MRCI method is well implemented in Molpro program, we perform MRCI energy corrections at selected CASSCF geometries to check how accurate is for the present CASSCF quantum level.

The initial condition of trajectories is started from Franck-Condon region of cis-azobenzene, and initial coordinates and velocities are set up by the following procedure. Firstly, we perform frequency calculation at equilibrium geometry of S_0 state in cis-azobenzene to obtain the normal mode coordinates. Secondly, initial normal-mode coordinates and velocities of trajectory are selected according to Wigner[34] distribution around S_0 state. Finally, these initial normal-mode coordinates and velocities are converted into Cartesian coordinates and velocities, at which the vertical excitation energy to selected excited state (S_2 or S_3 for the $\pi\pi^*$ excitation) is computed. The thermal kinetic energy with T=300K is added to all sampling trajectories with randomly distributing into initial Wigner velocities. Following the previous investigation in S_1 states, the 0.5 fs time-step size is selected in the entire simulation of trajectory from beginning to end and its validity was carefully checked.[9] For trajectories starting from both S_2

and S_3 states of cis-azobenzene, the time limit is set up as 1000 fs (if the trajectory stay in S_1

states until then, an additional 500 fs will be extended). The trajectories initiated from S_2 and

S_3 states are accounted as resonance if they are still in the S_2 state beyond 600fs and in the S_3

state beyond 750fs without experiencing any attempted hopping event.

3. Results and Discussion

Within ab initio quantum chemistry method at 5SA-CASSCF(6,6)/6-31G, we first optimized

geometries of all local minima, transition states, and conical intersections on all four low-lying

electronic states (S_0, S_1, S_2, and S_3). Atom numbering is given in Fig. 1. The most important

geometry parameters related with isomerization are summarized in Table 1; NN and two CN

bond lengths, two NNC bond angles (NNC_2 and NNC_{14}), CNNC and two NNCC dihedral

angles ($C_{19}C_{14}N_{13}N_1$ and $N_{13}N_1C_2C_7$). Potential energy profiles related to all the optimized

geometries are plotted in Fig. 2. On the potential energy surface of the ground-state (S_0) from

trans-azobenzene (trans S_0, CNNC=180°and E=0.0eV) to cis-azobenzene (cis S_0, CNNC=9.5°

and E=0.83eV), we found three transition states; planar inversion (TS-planar-inv S_0,

CNNC=0.0° and E=2.28eV), the rotation (TS-rot S_0, CNNC=81.2° and E=2.22eV) and the

inversion-assisted rotation (TS-inv-rot S_0, CNNC=49.3° and E=2.05eV). On the potential

energy surface of the first excited state (S_1), we found two transition states; TS-planar-inv S_1

(CNNC=0.0° and E=3.14eV) and TS-rot S_1 (CNNC=122.9° and E=2.96eV). On the potential

energy surface of the second excited state (S_2), we found two transition states; TS-rot-a S_2

(CNNC=97.6° and E=4.40eV) and TS-rot-b S_2 (CNNC=159.3° and E=4.96eV), besides there

is local minimum rot S_2 (CNNC=95.7° and E=3.94eV) in which trajectories can be trapped in

the dynamical simulation. On the potential energy surface of the third excited state (S_3), we

found no transition state, but there is local minimum rot S_3 (CNNC=95.1° and E=4.98eV) in

which trajectories can be trapped too. The calculated vertical excitation energies are in reasonable agreement with experiment;[35-37] the calculated ones to the S_1 and S_2 states at cis-isomer (trans-isomer) are 2.92eV and 5.25eV (3.08eV and 5.80eV) in comparison with experimental results 2.92eV and 4.40eV (2.82eV and 4.12eV). The present calculation with 5SA-CASSCF(6,6)/6-31G method agrees with the previous calculation with 2SA-CASSCF method for the S_0 and S_1 state.[9] Although the transition states roughly present the adiabatic isomerization pathways on their adiabatic potential energy surfaces, the conical intersections are the key to understand nonadiabatic isomerization pathways. We found two conical intersections between the S_0 and S_1 states; the rotation-type (CI-rot S_0/S_1, CNNC=97.4° and E=2.78eV) and inversion-type (CI-inv S_0/S_1, CNNC=180° and E=3.31eV). We found four conical intersections between the S_1 and S_2 states; CI-rot-a S_1/S_2 (CNNC=61.1° and E=4.67eV), CI-rot-b S_1/S_2 (CNNC=132° and E=4.73eV), cis-isomer-like (CI-cis S_1/S_2, CNNC=27.7° and E=5.22eV) and trans-isomer-like (CI-trans S_1/S_2, CNNC=180° and E=4.89eV). These four conical intersections actually play key role to govern isomerization mechanism after $\pi \rightarrow \pi^*$ excitation. We found one conical intersection between the S_2 and S_3 states; CI-rot S_2/S_3 (CNNC=93.1° and E=4.56eV), and this is optimized one. However, there are wide regions in which S_2 and S_3 states are very close together in energy and we found in dynamical simulation that trajectories hopping can take place in the wide region of configuration space between S_2 and S_3 states. These conical intersections coupled with all transition states and local minima exhibit complicated intermediate photoisomerization processes and eventually affect quantum yields, lifetimes and resonance intermediates for azobenzene photoisomerization. The Cartesian coordinates for all optimized structures (including conical intersections) are given in the Supporting Information (Section S4).

We selected the optimized geometries of cis S_0 and trans S_0, two minima rot S_2 and rot S_3, and all seven conical intersections from Table 1 to perform MRCI correction for vertical

excitation/de-excitation energies in comparison with the corresponding energies calculated from 5SA-CASSCF(6,6)/6-31G. As shown in Table 2, the vertical excitation/de-excitation energies calculated from both methods are in the same ordering for five singlet low-lying electronic states. At seven conical intersections, the corresponding energy differences between MRCI and CASSCF calculations are well kept within about 0.3eV except for CI-rot-a S_1/S_2, and this means it would have not so much geometries difference if we could optimize these seven conical intersections by MRCI method. Therefore, we expect that the present 5SA-CASSCF(6,6)/6-31G quantum level can be fairly accurate method to perform on-the-fly nonadiabatic trajectory simulation, especially for quite averaged observables such as quantum yields and lifetimes.

3.1 Topology of conical intersections among four low-lying excited states

Topology of seam surface for each conical intersection can be very different from one to another, and this affects photoisomerization mechanism upon the $\pi\pi^*$ excitation. We scan two-dimensional potential energy surfaces to demonstrate characters of each conical intersection zone. As azobenzene has been well studied theoretically, it is well-known that the photoisomerization proceeds via torsion of central CNNC moiety and planar inversion of NNC angles either independently or simultaneously, or via hybridizations of torsion and inversion motions. We need explore topology of conical intersections in terms of the torsion and inversion coordinates before performing large scale on-the-fly nonadiabatic trajectory simulation. For rotation-type isomerization pathway, two dihedral angles CNNC and NNCC are most important variables. For inversion-type isomerization pathway, two bond angles NNC1 and NCC2 are most important variables. We discuss two isomerization

pathways separately in the following by plotting contour map of potential-energy

difference between two adjacent potential energy surfaces. All corresponding three-

dimensional potential energy surfaces are plotted in Fig. S1 of Supplementary Information.

For the rotation pathway, we first construct one-dimensional coordinate by linear

interpolation of internal coordinates (LIIC)[38] between cis S_0 and the rotation-type CI, and

then between the rotation-type CI and trans S_0. This one dimension is plotted as horizontal

axis in Fig. 3a, Fig. 3c and Fig. 3e, and then the other dimension as vertical axis is

constructed by rotating two NNCC dihedral angles ($C_{19}C_{14}N_{13}N_1$ and $N_{13}N_1C_2C_7$)

simultaneously in opposite direction from $+90°$ to $-90°$. Finally, we have contour maps of

potential-energy difference as function of the CNNC and NNCC dihedral angles. Fig. 3a

shows a regular cone for CI-rot S_0/S_1; the potential energy gap between the S_0 and S_1 states

is far apart quickly in CNNC rotation direction and this means trajectories hopping happen

in local rotation region, while it varies slowly in NNCC rotation direction with maximum

separation about 0.5eV. Fig. 3c shows localized pattern for both CI-rot-a S_1/S_2 and CI-rot-b

S_1/S_2; these two are connected in CNNC rotation direction and this means trajectories

hopping happen in wide rotation region, while in NNCC rotation direction the potential

energy gap between the S_1 and S_2 states is far apart quickly. CI-rot-a S_1/S_2 and CI-cis S_1/S_2

are interacted each other so that it makes a complicated irregular pattern of conical

intersection as shown in cis-isomer zone of Fig. 3c. Fig. 3e shows a regular cone for CI-rot

S_2/S_3, but there is rotation path in which the potential energy gap between the S_2 and S_3

states is small all the way from cis-isomer zone to trans-isomer zone. This means that photo

excitation to S_3 state can undergo a rapid de-excitation to S_2 state anywhere

nonadiabatically, and this is confirmed from the present trajectory surface hopping

simulation.

For the inversion pathway, we chose initial internal coordinates at a fixed structure near each inversion conical intersection from where all internal coordinates are fixed except for NNC1 and NNC2 being independently scanned from +90° to 180° as shown in Fig. 3b, Fig. 3d and Fig. 3f. Finally, we have contour maps of potential-energy difference as function of the NNC1 and NNC2 bond angles. Fig. 3b shows the contour map around CI-inv S_0/S_1 with initial structure fixed at trans S_0, and it shows a regular localized cone in trans-isomer zone. Fig. 3d shows contour map around CI-trans S_1/S_2 with initial structure fixed at around CI-trans S_1/S_2, and it shows a regular localized cone as well. There is no optimized inversion conical intersection between the S_2 and S_3 states, but we make the contour map with initial structure fixed at trans S_0; Fig. 3f shows wide degenerate region between these two states and this means that photo excitation to S_3 state can undergo a rapid de-excitation to S_2 state anywhere nonadiabatically.

Based on the discussion mentioned above, we could present an intuitive point of view about global photoisomerization pathways. All isomerization mechanisms are initially generated by the CNNC and NNCC torsion motions after photo excited up to $\pi\pi^*$ band states for cis-azobenzene. Upon photo excitation to S_3 state from Franck-Condon region, the cis-azobenzene undergoes fast de-excitation to S_2 state within the first few femtoseconds. Either photo excitation to S_2 state directly or indirectly from S_3 state is the almost same, the cis-azobenzene from Franck-Condon region first visits the CI-cis S_1/S_2 conical intersection zone at CNNC angle in the region of [25°-45°]. If this attempted hopping fails, it goes another CI-rot-a S_1/S_2 conical intersection zone at CNNC angle in the region of [55°-80°]. If this attempted hopping fails again, it can traps in potential well at rot S_2 local minimum (CNNC=95.7°) in the S_2 state as intermediate resonance. Then, three different isomerization pathways follow; swing

back to CI-rot-a S_1/S_2, swing forward to CI-rot-b S_1/S_2, or staying in the well as long lifetime resonance. As the result from these three competing processes, the system stays in S_2 state much longer than in S_3 state, besides both slow and fast de-excitation from S_2 to S_1 state can happen easily. Once successful hopping to S_1 state is achieved, there are two isomerization pathways to S_0 state through CI-rot S_0/S_1 (in the previous study photo excitation to S_1 state, this is only pathway simulated) or CI-inv S_0/S_1 (in the present simulation, it takes place but still rare case). More detailed photo isomerization mechanisms can be obtained from the following on-the-fly trajectory surface hopping simulation involving in these conical intersection networks.

We have run 336 trajectories starting from vertical excitation to Franck-Condon region on S_2 state; 97 reactive (131 nonreactive) ones end up to trans (cis) S_0 with 108 resonance trajectories terminating in S_2 rot potential well. We have run 200 trajectories starting from vertical excitation to Franck-Condon region on S_3 state; 64 reactive (87 nonreactive) ones end up to trans (cis) S_0 with 49 resonance trajectories terminating in S_2 rot potential well. Based on total 536 sampling trajectories, we classify the six typical isomerization schemes corresponding to related typical trajectories (both reactive and nonreactive). We discuss isomerization mechanisms separately for cis-azobenzene starting from S_2 and S_3 states in the following.

Before leaving this subsection, we would like to mention about how to search conical intersections. For the present well-studied azobenzene molecule, we know a few dihedral angles governing torsion and inversion motions are responsible for conical intersections, and thus we plot contour map in terms of these dihedral angles for energy difference between involved two states. Then, we can locate configuration geometry very close to conical intersection from which we do optimization with well implemented method in Moplro program for instance. Actually, CI-cis S1/S2 and CI-trans S1/S2 are found from this procedure. For the

general case, we can do preliminary on-the-fly trajectory simulation with the lower level ab initio method, and then we calculate energy difference between involved two states along the sampling trajectories and locate configuration geometry very close to conical intersection. Actually, CI-rot-a S1/S2 and CI-rot-b S1/S2 are found from this way.

3.2 Photoisomerization mechanisms starting from S_2 state

Photoisomerization mechanism of cis-1 case. The cis-1 case is defined by reactive (nonreactive) trajectories starting from Franck-Condon region experiencing the following consecutive processes; cis S_0-S_2VEE (VEE means vertical excitation energy E=6.08eV as shown in Fig. 2) →CI-cis S_1/S_2→CI-rot S_0/S_1→ trans (cis) S_0 as shown in Scheme(a). The first step is fast internal conversion around~10 fs upon to CI-cis S_1/S_2 and the second step is about 10fs to 100fs upon to CI-rot S_0/S_1. Once trajectories are in S_1 state, the rest of processes continue with CNNC and NNCC torsion motion same as those observed in the previous work.[9] This cis-1 case is in lifetime about 200 femtoseconds. Fig. 4 shows a typical reactive (nonreactive) trajectory that takes 10.5 (9.0) fs to CI-cis S_1/S_2 and 50.5 (70.0) fs to CI-rot S_0/S_1 with overall nonadiabatic switching probability 0.71 (0.71) from cis S_0-S_2VEE to CI-rot S_0/S_1. The motions of two NNC bond angles plus one CNNC and four NNCC dihedral angles are vibration with small amplitude as shown in Fig. 4. We conclude that cis-1 case is two-step fast-fast photoisomerization process.

Photoisomerization mechanism of cis-2 case. The cis-2 case is defined by reactive (nonreactive) trajectory following consecutive processes; cis S_0-S_2VEE→CI-rot-a S_1/S_2→CI-rot S_0/S_1→ trans (cis) S_0 as shown in Scheme(b). The cis-2 case is similar to cis-1 case except the first step is internal conversion around~25 fs upon to CI-rot-a S_1/S_2. This cis-2 case is also in lifetime about 200 femtoseconds. Fig. 5 shows a typical reactive

(nonreactive) trajectory that takes 23.5 (21.5) fs to CI-rot-a S_1/S_2 and 52.5 (84.0) fs to CI-rot S_0/S_1 with overall nonadiabatic switching probability 0.80 (0.92) from cis S_0-S_2VEE to CI-rot S_0/S_1.Dihedral angles CNNC and synchronous NNCC motions dominate the isomerization process, while the NNC motions oscillate nonsymmetrically in region of [110°-140°]. We conclude that cis-2 case is also two-step fast-fast photoisomerization process.

Photoisomerization mechanism of cis-3 case. The cis-3 case is defined by reactive (nonreactive) trajectory following consecutive processes; cis S_0-S_2VEE→rot S_2→ CI-rot-a S_1/S_2 →CI-rot S_0/S_1→ trans (cis) S_0 as shown in Scheme(c). In this case, trajectories failed in hopping at CI-cis S_1/S_2 and CI-rot-a S_1/S_2 can be trapped in the local potential well rot S_2 for about 100fs to 900fs, and then swing back to CI-rot-a S_1/S_2. Obviously, the trajectory trapping into potential well affects lifetime and it is usually several times longer than cis-1 and cis-2 cases. Fig. 6 shows that a typical reactive (nonreactive) trajectory traps in the well until 569fs (122fs) before hopping via CI-rot-a S_1/S_2, and then 608.5 (151.5) fs to CI-rot S_0/S_1 with overall nonadiabatic switching probability 0.66 (0.34) from cis S_0-S_2VEE to CI-rot S_0/S_1. Dihedral angle CNNC firstly oscillates around 90° for about 100fs, then increase to around ~120° and decrease to ~60°. Moreover, the NNCC angles which reflect the torsion of benzene ring oscillate around 0° and 180° and this torsion motion is needed for trajectory visiting both CI-rot-a S_1/S_2 and CI-rot-b S_1/S_2. We conclude that cis-3 case is two-step slow-fast photoisomerization process.

Photoisomerization mechanism of cis-4 case. The cis-4 case is defined by reactive (nonreactive) trajectory following consecutive processes; cis S_0-S_2VEE→rot S_2→ CI-rot-b S_1/S_2 →CI-rot S_0/S_1→ trans (cis) S_0 as shown in Scheme(d). The cis-4 case is very similar

to cis-3 and it does trap in potential well rot S_2 for long lifetime. In this case, trajectories visit CI-rot-b S_1/S_2 that is close to trans-isomer (trans S_2) region, so that the prolonged lifetime on trans S_1 state is also observed as the trajectories go the other end of rotation path and then back to the CI-rot S_0/S_1 region. This simulated mechanism is actually observed in the recent transient experiment of Quick et. al.,[24] and they proposed that the cis-azobenzene could isomerize to trans via an S_n/S_1 conical intersection, and resulting in a mixed cis/trans S_1 population. That is why both reactive and nonreactive trajectories can have long lifetime as shown in Fig. 7, and this is especially shown for the nonreactive trajectory that the CNNC angle increases to 180° before hopping to S_1. Fig. 7 shows that a typical reactive (nonreactive) trajectory traps in the well until 311.5fs (414.5fs) before hopping via CI-rot-b S_1/S_2, and then 1565.5 (531.0) fs to CI-rot S_0/S_1 with overall nonadiabatic switching probability 0.25 (0.67) from cis S_0-S_2VEE to CI-rot S_0/S_1. We conclude that cis-3 case is two-step slow-slow photoisomerization process.

Upward trajectory hopping from S_2 to S_3 state: Along both rotation and inversion isomerization pathways (see Fig. 3e and Fig. 3f), there exists wide region in which potential energy gap between S_2 and S_3 states is very small all the way from cis-isomer to trans-isomer region. Trajectories initially starting from Franck-Condon region of S_2 state can have chance to experience upward hopping to S_3 state and then back to S_2 state. Actually no matter how trajectories follow $S_2 \rightarrow S_3 \rightarrow S_2$ isomerization pathway, once they are back to S_2 state, the following $S_2 \rightarrow S_1 \rightarrow S_0$ processes show the same isomerization mechanism as mentioned above.

However, we observe if trajectories hop back to S_2 state along rotation pathway, they finish within about 5fs via CI-cis region or about 20fs via CI-rot S_2/S_3 region, and the following $S_2 \rightarrow S_1 \rightarrow S_0$ processes could follow four cases (cis-1, cis-2, cis-3, and cis-4)

mentioned above. If trajectories hop back to S_2 state along inversion pathway, they stay on S_3 state in much longer time. A typical nonreactive trajectory shown in left panel of Fig. 8 hops up to S_3 state at 0.5fs, back to S_2 state via CI-rot S_2/S_3 at 21.0fs, down to S_1 state via CI-cis S_1/S_2 at 21.5fs, and finally down to S_0 state via CI-rot S_0/S_1 at 53.0fs. This nonreactive trajectory belongs to cis-1 case of photoisomerization. A typical reactive trajectory shown in right panel of Fig. 8 hops up to S_3 state at 62.5fs, back to S_2 state via CI-rot S_2/S_3 at 81.0fs, down to S_1 state via CI-rot-a S_1/S_2 at 83.0fs, and finally down to S_0 state via CI-rot S_0/S_1 at 121.5fs. This reactive trajectory belongs to cis-3 case of photoisomerization. However, this typical nonreactive (reactive) trajectory propagates from cis S_0-S_2VEE to CI-rot S_0/S_1 with overall nonadiabatic switching probability 0.13 (0.17).

In brief summary, the cis-1 and cis-2 cases compose two-step fast-fast photoisomerization pathways in which system experiences transient S_2 state and then down to S_1 state with a little bit slow process, and this depends on the numbers of swings around CI-rot S_0/S_1. Finally, trajectories reach S_0 state from the lifetime several tenths to hundred femtoseconds. Simulated lifetime from the cis-1 and cis-2 cases agree with the time constant of 0.1ps for S_2 and S_1 processes observed by Satzger et. al. experimentally.[22] On the other hand, the cis-3 case composes two-step slow-fast photoisomerization pathways with trajectories trapping only in rot S_2 potential well, while cis-4 case compose two-step slow-slow photoisomerization pathways with trajectories trapping in both rot S_2 and trans S_1 potential wells. Finally, trajectories reach S_0 state from the lifetime several hundreds to thousand femtoseconds. The cis-3 and cis-4 cases agree with the lifetime observed by Quick et. al.[24] in the recent transient experiment as well. According the results from the present simulation, we conclude that the rotation pathway governed by the CNNC and NNCC torsion motion dominates the cis-azobenzene photoisomerization, while the inversion pathway governed by the NNC symmetrical and nonsymmetrical motion can influence photoisomerization to some extent.

This inversion pathway is actually similar to a weakly inversion assisted rotation. Based on the semiempirical nonadiabatic molecular dynamics simulation including solvent and decoherence effect, Persico and coworkers[13, 28, 29] have proposed that for the $\pi\to\pi^*$ isomerization mechanism the torsion motion of N=N bond plays most important role in both vacuum and solvent environment. We here present more detailed intermediate isomerization processes on how trajectories follow complicated conical intersection network. In the comparison to $n\to\pi^*$ isomerization, the drop of quantum yields in $\pi\to\pi^*$ case is mainly attributed to trajectories trapping into the rot S_2 potential well and this is considered as the inertia effects of reactants.[13] Finally, we should mention that there are quite amount resonant trajectories in the present simulation and one of them is given in Fig. S2 of Supporting Information.

3.3 Photoisomerization mechanisms starting from S_3 state

For the trajectories starting from S_3 state, once they hop down to S_2 state and most of them basically follow the four cases mentioned above like trajectories starting from S_2 state. These trajectories do not present new photoisomerization mechanism and we just give some of sampling trajectories corresponding to cis-1, cis-2, cis-3, and cis-4 in Fig. S3 to Fig. S6 of Supporting Information. However, we do find the two new cases discussed in the following.

Photoisomerization mechanism of cis-5 case: The cis-5 case is defined by reactive trajectory following consecutive processes; one is cis S_0-S_3VEE (vertical excitation energy E=6.22eV as shown in Fig. 2)→cis FC S_2 →rot S_2→ CI-trans S_1/S_2 and the other is cis S_0-S_3VEE→ rot S_3→ CI-rot-a S_2/S_3 →rot S_2→CI-trans S_1/S_2 as shown in Scheme(e). We do not find that any trajectory starting from S_2 state visits CI-trans S_1/S_2 region, so this is new case of photoisomerization pathway. Vertical excitation energy on S_3 state is 0.14eV higher than S_2 state, and we believe this is key factor for trajectories to visit CI-trans S_1/S_2 region. Then, the present cis-5 trajectories bifurcate into two pathways; one is hopping down to S_0 state via CI-

rot S_0/S_1 and the other via CI-inv S_0/S_1. The latter case is for the first time to prove from direct simulation in which the cis-azobenzene photoisomerization upon $\pi \rightarrow \pi^*$ excitation can hop down to the ground state via the inversion conical intersection. This is because that present simulation at CSSCF quantum chemistry level can accurately describe global landscape of excited-state potential energy surfaces coupled into conical intersection network. The trajectories continue NNC inversion motion on S_1 state at a semi-planar trans form geometry with both NNC angles larger than 145° followed by hopping down S_0 state via CI-inv S_0/S_1 region, and then they can only go trans-isomer product. Surprisingly, the trajectories visits CI-trans S_1/S_2 followed rotation pathway to S_0 state via CI-rot S_0/S_1 also end up with trans-isomer product. This means once trajectories visit CI-trans S_1/S_2 region, the certain memory effect of trans form geometry makes trajectories in favor of trans-azobenzene product. Fig. 9 shows two typical reactive trajectories; one (left panel in Fig. 9) follows CI-inv S_0/S_1 region hopping at CNNC =161° with lifetime 1080.5fs and overall nonadiabatic switching probability 0.59, and the other (right panel in Fig. 9) follows CI-rot S_0/S_1 region hopping at CNNC = -107° with lifetime 481fs and overall nonadiabatic switching probability 0.40. In both reactive isomerisation cases, four NNCC dihedral angles vibrate with large amplitude of motion along reactive pathways. We conclude that cis-5 case is three-step fast-slow-slow photoisomerization process. The cis-5 shows that CI-trans S_1/S_2 provides a peculiar new isomerisation mechanism.

Photoisomerization mechanism of cis-6 case: The cis-6 case is defined by reactive (nonreactive) trajectory following consecutive processes; cis S_0-S_3VEE$\rightarrow$ rot $S_3$$\rightarrow$ CI-rot-a S_2/S_3 $\rightarrow$rot S_2 $\rightarrow$CI-rot-a S_1/S_2 (or CI-rot-b S_1/S_2) $\rightarrow$CI-rot $S_0/S_1$$\rightarrow$ trans (cis) S_0 as shown in Scheme(f). Trajectories trapping in rot S_3 potential well are usually in short time less than 100fs because of existing wide region of conical seam surface between the S_2 and S_3 states. The new point of this case is due to this short trapping in rot S_3 potential well and then following step is very much like cis3 or cis-4 case. Consecutive trapping in rot S_2 potential

well can be either short or relatively long time depending on NNC motion. Fig. 10 shows a reactive (nonreactive) trajectory follows CI-rot-a S_1/S_2 (CI-rot-b S_1/S_2) region hopping at CNNC $=51°$ (CNNC $=121°$) with lifetime 849fs (517fs) and overall nonadiabatic switching probability 0.71(0.15). For the trajectories starting from S_3 state, we observe most of the trans intermediate in favor of staying in S_2-state potential well, and for the trajectories starting from S_2 state, we observe most of the trans intermediate in favor of staying in S_1-state potential well that is in agreement with experimental measurement.[24] Theoretically, this is consistent with that trajectory with higher kinetic energy traps in the potential well with longer lifetime because of dynamical spreading of resonance motion.

4. Concluding remarks

Based on our newly developed nonadiabatic molecular dynamics method to compute global nonadiabatic switching probability by only using electronic adiabatic potential energy surfaces and its gradients, we could be able to perform on-the-fly trajectory surface hopping algorithm at the CASSCF ab initio quantum level to probe $\pi\pi^*$ photoisomerization mechanism of the azobenzene within four singlet low-lying electronic states coupled with complicated conical intersection network. The computational cost in the present method is the same for two states or more than two states with use of on-the-fly trajectory surface hopping method. We have performed 536 sampling trajectories (336 from S_2 and 200 from S_3) starting from cis-azobenzene, we can estimate total reactive quantum yield about 0.3~0.45 and here 0.45 comes from if we count half of resonance trajectories finally approaching to product region at trans S_0. This is in very close agreement with recent experiment results 0.24~0.50.[5] Another advantage with the present global switching algorithm is that we can estimate overall nonadiabatic transition probability for each sampling trajectory from the beginning to the end. An immediate

application is that from given 8 typical reactive trajectories mentioned above (from Fig. 4 to Fig. 10), we obtain reactive quantum yield as $(0.71+0.80+0.66+0.25+0.17+0.40+0.59+0.71)/8$ = 0.53 which is not bad in comparison with the one estimated from 536 sampling trajectories. This means that the present global switching algorithm can provide a computationally fast converged method with much less number of sampling trajectories in the nonadiabatic molecular dynamic simulation.

Photoisomerization mechanism of azobenzene upon S_2 and S_3 $\pi\pi^*$ excitation is mostly determined by four conical intersections between S_1 and S_2 states, namely one close to cis-isomer CI-cis S_1/S_2, another close to trans-isomer CI-trans S_1/S_2, and two in the middle between cis and trans CI-rot-a S_1/S_2 and CI-rot-b S_1/S_2. From these four conical intersections plus other conical intersections between S_2 and S_3 states and between S_0 and S_1 states, we classified six cases to demonstrate detailed photoisomerization mechanism associated with 8 typical reactive trajectories and 6 typical nonreactive trajectories; two-step fast-fast photoisomerization processes have the lifetime from several tenths to hundred femtoseconds, two-step fast-slow and slow-slow photoisomerization processes have lifetime from the several hundreds to thousand femtoseconds. Trajectories have long lifetime mostly depending on the trapping in the potential well rot S_2 on the S_2 state. Comparison with four localized conical intersections between S_1 and S_2 states, the conical intersections between S_2 and S_3 states are very much delocalized with spreading over all place along both rotation and inversion pathways from ci-isomer to trans-isomer and this is why that trajectories starting from S_3 state hop down to S_2 state within the tenth femtoseconds even if there is potential well rot S_3 on S_3 state. It is interesting to note that CI-trans S_1/S_2 has peculiar property, and trajectories visiting this conical intersection always result into trans product no mater via CI-rot S_0/S_1 or CI-inv S_0/S_1. This is

regarded as a mixed rotation-inversion isomerization process. Finally, we believe that the present trajectory-based on-the-fly nonadiabatic simulation provides a complete photoisomerization mechanism of the cis-azobenzene upon to $\pi\pi^*$ excitation.

Actually Landau-Zener analytical switching probability was utilized to study the charge transfer reaction in the DH_2^+ system in the early 1970s by Tully and Preston, [39] and later this reaction calculation was improved by employing Zhu-Nakamura formula for cumulative probability [40] and cross section.[41] However, these studies require predetermining seam surface between two adiabatic potential energy surfaces and it is not applicable to big system. The present new algorithm does not need any information about seam surface and that is why we can now study big system. On the other hand, we notice that trajectory-based on-the-fly surface hopping algorithm can be applied to photochemistry in the situation of both conical intersection and intersystem crossing.[42,43] With analytically generalized global switching probability for general crossing and noncrossing nonadiabatic transitions developed by Zhu,[44] the present method can also be straightforward to be applied for intersystem crossing.

Acknowledgements

References

1. W. Szymański, J. M. Beierle, H. A. V. Kistemaker, W. A. Velema and B. L. Feringa, *Chem. Rev.,* 2013, **113**, 6114.

2. Z. F. Liu, K. Hashimoto and A. Fujishima, *Nature,* 1990, **347**, 658.

3. P. H. Rasmussen, P. S. Ramanujam, S. Hvilsted and R. H. Berg, *J. Am. Chem. Soc.,* 1999, **121**, 4738.

4. Y. Norikane and N. Tamaoki, *Org. Lett.,* 2004, **6**, 2595.

5. T. Muraoka, K. Kinbara and T. Aida, *Nature,* 2006, **440**, 512.

6. Y. Kim, J. A. Philips, H. Liu, H. Kang and W. Tan, *Proc. Natl. Acad. Sci. USA,* 2009, **106**, 6489.

7. M. R. Banghart, A. Mourot, D. L. Fortin, J. Z. Yao, R. H. Kramer and D. Trauner, *Angew. Chem. Int. Ed.,* 2009, **48**, 9097.

8. H. M. D. Bandara and S. C. Burdette, *Chem. Soc. Rev.,* 2012, **41**, 1809.

9. L. Yu, C. Xu, Y. Lei, C. Zhu and Z. Wen, *Phys. Chem. Chem. Phys.,* 2014, **16**, 25883.

10. A. J. Neukirch, L. C. Shamberger, E. Abad, B. J. Haycock, H. Wang, J. Ortega and O. V. Prezhdo, J. P. Lewis, *J. Chem. Theory Comput.,* 2014, **10**, 14.

11. O. Weingart, Z. Lan, A. Koslowski and W. Thiel, *J. Phys. Chem. Lett.,* 2011, **2**, 1506.

12. M. Pederzoli, J. Pittner, M. Barbatti and H. Lischka, *J. Phys. Chem. A,* 2011, **115**, 11136.

13. T. Cusati, G. Granucci and M. Persico, *J. Am. Chem. Soc.,* 2011, **133**, 5109.

14. Y. Ootani, K. Satoh, A. Nakayama, T. Noro and T. Taketsugu, *J. Chem. Phys.,* 2009, **131**, 194306.

15. I. K. Lednev, T. Q. Ye, R. E. Hester and J. N. Moore, *J. Phys. Chem.,* 1996, **100**, 13338.

27

16.   I. K. Lednev, T. Q. Ye, P. Matousek, M. Towrie, P. Foggi, F. V. R. Neuwahl, S. Umapathy, R. E. Hester and J. N. Moore, *Chem. Phys. Lett.,* 1998, **290**, 68.

17.   T. Nägele, R. Hoche, W. Zinth and J. Wachtveitl, *Chem. Phys. Lett.,* 1997, **272**, 489.

18.   J. Azuma, N. Tamai, A. Shishido and T. Ikeda, *Chem. Phys. Lett.,* 1998, **288**, 77.

19.   T. Fujino and T. Tahara, *J. Phys. Chem. A,* 2000, **104**, 4203.

20.   T. Fujino, S. Y. Arzhantsev and T. Tahara, *J. Phys. Chem. A,* 2001, **105**, 8123.

21.   H. Satzger, S. Spörlein, C. Root, J. Wachtveitl, W. Zinth and P. Gilch, *Chem. Phys. Lett.,* 2003, **372**, 216.

22.   H. Satzger, C. Root and M. Braun, *J. Phys. Chem. A,* 2004, **108**, 6265.

23.   T. Schultz, J. Quenneville, B. Levine, A. Toniolo, T. J. Martinez, S. Lochbrunner, M. Schmitt, J. P. Shaffer, M. Z. Zgierski and A. Stolow, *J. Am. Chem. Soc.,* 2003, **125**, 8098.

24.   M. Quick, A. L. Dobryakov, M. Gerecke, C. Richter, F. Berndt, I. N. Ioffe, A. A. Granovsky, R. Mahrwald, N. P. Ernsting and S. A. Kovalenko, *J. Phys. Chem. B,* 2014, **118**, 8756.

25.   P. Sauer and R. E. Allen, *Chem. Phys. Lett.,* 2008, **450**, 192.

26.   J. Shao, Y. Lei, Z. Wen, Y. Dou and Z. Wang, *J. Chem. Phys.,* 2008, **129**, 164111.

27.   Y. Dou, Y. Hu, S. Yuan, W. Wu and H. Tang, *Mol. Phys.,* 2009, **107**, 181.

28.   C. Ciminelli, G. Granucci and M. Persico, *Chem. Eur. J.,* 2004, **10**, 2327.

29.   V. Cantatore, G. Granucci and M. Persico, *Comput. Theor. Chem.,* 2014, **1040-1041**,126.

30.   L. Verlet, *Phys. Rev.,* 1967, **159**, 98.

31.   C. Zhu and H. Nakamura, *J. Chem. Phys.,* 1992, **97**, 8497.

32.   C. Zhu and H. Nakamura, *J. Chem. Phys.,* 1993, **98**, 6208.

28

33.   MOLPRO, a package of ab initio programs written by H.-J. Werner and P. J. Knowles,

Version 2009.1, G. Knizia, F. R. Manby, M. Schütz, et al.

34.   E. Wigner, *Phys. Rev.,* 1932, **40**, 749.

35.   D. L. Beveridge and H. H. Jaffé, *J. Am. Chem. Soc.,* 1966, **88**, 1948.

36.   J. A. Bouwstra, A. Schouten and J. Kroon, *Acta Cryst.,* 1983, C**39**, 1121.

37.   T. Tsuji, H. Takashima, H. Takeuchi, T. Egawa and S. Konaka, *J. Phys. Chem. A,* 2001, **105**,

9347.

38.   M. Merchán, L. Serrano-Andrés, M. A. Robb and L. Blancafort, *J. Am. Chem. Soc.,* 2005,

127, 1820.

39.   J. C. Tully and R. K. Preston, *J. Chem. Phys.* 1971, **55**, 562.

40.   C. Zhu, H. Kamisaka, and H. Nakamura, *J. Chem. Phys.,* 2002, **116**, 3234.

41.   B. Li and K.-L. Han, *J. Chem. Phys.,* 2008, **128**, 114116.

42.   L. Martinez-Fernandez, I. Corral, G. Granucci and M. Persico, *Chem. Sci.,* 2014, **5**, 1336.

43.   G. Cui and W. Thiel, *J. Chem. Phys.,* 2014, **141**, 124101.

44.   C. Zhu, *J. Chem. Phys.,* 1996, **105**, 4159.

Table 1 Optimized geometries and energies for equilibriums, transition states, and conical intersections in the ground state S_0 and the low-lying singlet excited S_1, S_2 and S_3 states. The energy of ground state trans minimum is selected as zero and the energies are given in eV. Bond length r is given in angstrom (Å), and bond angles and dihedral angles d are given in degrees.

Geometry	Energy	r_{NN}	r_{CN}	a_{NNC}	d_{CNNC}	d_{NNCC}
trans S_0	0.00	1.229	1.424/1.417	117.9/118.2	180.0	0.0/0.0
Expt [a]		1.260	1.427/1.427	113.6/113.6	180.0	0.0/0.0
cis S_0	0.83	1.231	1.430/1.430	126.3/126.3	9.5	46.5/46.5
Expt [b]		1.253	1.449/1.449	121.9/121.9	8.0	53.3/53.3
TS-inv-rot S_0	2.05	1.216	1.442/1.353	119.6/178.3	49.3	4.8/-175.2
TS-rot S_0	2.22	1.448	1.362/1.362	115.1/115.1	81.2	4.0/4.0
TS-planar-inv S_0	2.28	1.227	1.447/1.388	121.8/177.1	0.0	0.0/0.0
CI-rot S_0/S_1	2.78	1.235	1.410/1.356	121.7/149.1	97.4	179.9/-14.7
CI-inv S_0/S_1	3.31	1.207	1.332/1.332	150.8/150.8	180.0	0.0/0.0
trans S_1	2.38	1.245	1.364/1.388	131.7/130.7	180.0	0.0/0.0
cis S_1	3.47	1.211	1.363/1.363	149.6/149.6	0.0	0.0/0.0
TS-rot S_1	2.96	1.236	1.389/1.383	127.0/138.0	122.9	6.0/-23.8
TS- planar-inv S_1	3.14	1.222	1.368/1.371	136.1/167.5	0.0	-0.0/-0.0
CI-cis S_1/S_2	5.22	1.309	1.339/1.339	121.0/121.0	27.7	7.8/7.8
CI-rot-a S_1/S_2	4.67	1.310	1.349/1.349	121.0/121.0	61.1	-3.3/-3.3
CI-rot-b S_1/S_2	4.73	1.368	1.349/1.348	115.2/115.2	132.0	-4.1/-4.0
CI-trans S_1/S_2	4.89	1.340	1.380/1.380	111.0/111.0	180.0	0.0/0.0
trans S_2	5.01	1.205	1.358/1.358	156.9/156.9	180.0	0.0/0.0
rot S_2	3.94	1.237	1.383/1.383	130.8/130.8	95.7	-2.2/-2.2
TS-rot-a S_2	4.40	1.237	1.391/1.416	133.6/131.5	97.6	5.6/-97.7
TS-rot-b S_2	4.96	1.214	1.355/1.355	154.8/154.8	159.3	38.3/38.3
CI-rot -a S_2/S_3	4.56	1.330	1.401/1.407	118.8/118.6	93.1	1.2/-2.0
trans S_3	5.48	1.371	1.360/1.317	111.0/117.2	180.0	0.0/0.0
rot S_3	4.98	1.336	1.390/1.365	117.5/121.1	95.1	-4.2/-4.2

[a]Ref. 35, [b]Ref. 37.

Table 2. Vertical excitation/de-excitation energies calculated by 5SA-CASSCF(6,6)/6-31G and corrected by MRCI method at the CASSCF optimized geometries indicted in the first column. CASSCF (MRCI) energies are all relative to CASSCF (MRCI) trans-S_0 as zero of energy. All energies are given in eV.

Geometry	Method	Energy S_0	Energy S_1	Energy S_2	Energy S_3	Energy S_4
trans S_0	CASSCF	0.00	3.08	5.80	5.82	6.35
	MRCI	0.00	3.14	5.43	5.68	5.86
cis S_0	CASSCF	0.82	3.77	5.99	6.72	7.44
	MRCI	0.79	3.78	6.04	6.07	7.13
CI-rot S_0/S_1	CASSCF	2.78	2.78	4.81	5.78	6.02
	MRCI	2.68	2.84	4.67	5.74	5.99
CI-inv S_0/S_1	CASSCF	3.31	3.31	5.14	5.77	6.95
	MRCI	2.94	3.09	4.67	5.82	6.42
CI-cis S_1/S_2	CASSCF	4.27	5.22	5.22	7.65	8.44
	MRCI	4.42	4.79	5.09	7.45	7.96
CI-rot-a S_1/S_2	CASSCF	2.56	4.67	4.67	5.76	6.85
	MRCI	2.60	3.51	3.62	5.76	6.66
CI-rot-b S_1/S_2	CASSCF	1.44	4.73	4.73	5.16	6.17
	MRCI	1.49	4.32	4.59	4.98	5.90
CI-trans S_1/S_2	CASSCF	0.28	5.41	5.41	7.05	7.81
	MRCI	0.31	5.10	5.41	5.88	6.75
rot S_2	CASSCF	2.45	3.08	3.94	5.43	5.67
	MRCI	2.52	3.05	3.73	5.39	5.64
CI-rot -a S_2/S_3	CASSCF	2.24	3.86	4.56	4.56	5.96
	MRCI	2.39	3.75	4.29	4.66	5.93
rot S_3	CASSCF	2.28	4.18	4.78	4.98	5.55
	MRCI	2.38	4.00	4.44	4.95	5.53

Fig. 1 Atom numbering (geometry of rot-azobenzene in the S_2 state).

Fig. 2 Potential energy profiles for all sudden points in Table 1, VEE stands for vertical excitation energy.

Fig. 3 Counter plots of potential energy difference (in eV) between two adjacent adiabatic states with conical intersections distributing along rotation (left panel) and inversion (right panel) isomerization pathways; (a) and (b) between S_0 and S_1, (c) and (d) between S_1 and S_2, and (e) and (f) between S_2 and S_3.

Scheme Photoisomerization mechanism of cis-azobenzene starting from the Franck-Condon region on S_2 (a) cis-1, (b) cis-2, (c) cis-3 and (d) cis-4, and on S_3 (e) cis-5 and (f) cis-6.

Fig. 4 Potential energies and two NNC bond angles, CNNC and four NNCC dihedral angles evolve along trajectories in cis-1 case (see Scheme (a)). Left (right) panel is a reactive (nonreactive) trajectory: hopping via CI-cis S_1/S_2 for switching probability $p=$ 0.842 with $a^2=3.7$ and $b^2=5.6$ at 10.5fs ($p=0.71$ with $a^2=1.1$ and $b^2=4.4$ at 9.0fs), and then hopping via CI-rot S_0/S_1 for switching probability $p=0.84$ with $a^2=2.1$ and $b^2=9.0$ at 50.5fs ($p=0.999$ with $a^2=11281$ and $b^2=146$ at 72.0fs).

Fig. 5 The same as in Figure 4 except for cis-2 case (see Scheme (b)). Left (right) panel is a reactive (nonreactive) trajectory: hopping via CI-rot-a S_1/S_2 for switching probability $p=0.82$ with $a^2=3.1$ and $b^2=5.2$ at 23.5fs ($p=0.94$ with $a^2=23$ and $b^2=7.4$ at 21.5fs), and then hopping via CI-rot S_0/S_1 for switching probability $p=0.98$ with $a^2=36$ and $b^2=27$ at 52.5fs ($p=0.98$ with $a^2=89$ and $b^2=34$ at 84.0fs).

Fig. 6 The same as in Figure 4 except for cis-3 case (see Scheme (c)). Left (right) panel is a reactive (nonreactive) trajectory: hopping via CI-rot-a S_1/S_2 for switching probability $p= 0.92$ with $a^2=20.9$ and $b^2 =4.2$ at 569.0fs ($p= 0.998$ with $a^2=4631$ and $b^2 =44$ at 122fs), and then hopping via CI-rot S_0/S_1 for switching probability $p= 0.72$ with $a^2=0.79$ and $b^2 =7.3$ at 608.5fs ($p=0.34$ with $a^2=0.08$ and $b^2 =6.4$ at 151.5fs).

Fig. 7 The same as in Figure 4 except for cis-4 case (see Scheme (d)). Left (right) panel is a reactive (nonreactive) trajectory: hopping via CI-rot-b S_1/S_2 for switching probability $p= 0.72$ with $a^2=0.89$ and $b^2 =6.2$ at 311.5fs ($p= 0.8$ with $a^2=1.7$ and $b^2 =7.3$ at 414.5fs), and then hopping via CI-rot S_0/S_1 for switching probability $p= 0.34$ with $a^2=0.1$ and $b^2 =5.0$ at 1565.5fs ($p=0.84$ with $a^2=1.2$ and $b^2 =16$ at 531.0fs).

Fig. 8 The same as in Figure 4 except for upward hopping from S_2 to S_3 state. Left (right) panel is a nonreactive (reactive) trajectory in cis-1 (cis-3) case: hopping up via CI-rot S_2/S_3 for switching probability $p= 0.97$ with $a^2=167$ and $b^2 =5.5$ at 0.5fs ($p= 0.3$ with $a^2=0.24$ and $b^2 =1.6$ at 62.5fs), hopping down via CI-rot S_2/S_3 for switching probability $p= 0.94$ with $a^2=27.6$ and $b^2 =5.5$ at 21.5fs ($p= 0.98$ with $a^2=109$ and $b^2 =14.8$ at 81fs), hopping down via CI-cis S_1/S_2 (CI-rot-a S_1/S_2) for switching probability $p= 0.99$ with $a^2=500$ and $b^2 =19.5$ at 22fs ($p= 0.6$ with $a^2=0.63$ and $b^2 =3.7$ at 83fs), and then hopping down via CI-rot S_0/S_1 for switching probability $p= 0.138$ with $a^2=0.03$ and $b^2 =5.0$ at 53fs ($p=0.97$ with $a^2=44$ and $b^2 =20$ at 121.5fs).

Fig. 9 The same as in Figure 4 except for cis-5 case (see Scheme (e)). Left (right) panel is a reactive (reactive) trajectory: hopping via CI-rot-a S_2/S_3 (CI-cis S_2/S_3) for switching probability $p= 0.68$ with $a^2=0.8$ and $b^2 =5.2$ at 32fs ($p= 0.98$ with $a^2=109$ and $b^2 =16$ at 11fs), hopping via CI-trans S_1/S_2 for switching probability $p= 0.88$ with $a^2=5.3$ and $b^2 =7.6$ at 333.5fs ($p= 0.78$ with $a^2=5.3$ and $b^2 =2.0$ at 346.5fs), and then hopping via CI-inv S_0/S_1 (CI-rot S_0/S_1) for switching probability $p= 0.99$ with $a^2=137$ and $b^2 =55$ at 1080.5fs ($p=0.52$ with $a^2=0.18$ and $b^2 =7.7$ at 481.0fs).

Fig. 10 The same as in Figure 4 except for cis-6 case (see Scheme (f)). Left (right) panel is a reactive (nonreactive) trajectory: hopping via CI-rot-a S_2/S_3 for switching probability $p=0.99$ with $a^2=916$ and $b^2=18$ at 22.5fs ($p=0.70$ with $a^2=0.93$ and $b^2=5.1$ at 90fs), hopping via CI-rot-a S_1/S_2 (CI-rot-b S_1/S_2) for switching probability $p=0.73$ with $a^2=1.8$ and $b^2=3.5$ at 748fs ($p=0.28$ with $a^2=0.15$ and $b^2=2.4$ at 506.5fs), and then hopping via CI-rot S_0/S_1 for switching probability $p=0.98$ with $a^2=56$ and $b^2=41$ at 849fs ($p=0.76$ with $a^2=0.6$ and $b^2=12$ at 517fs).
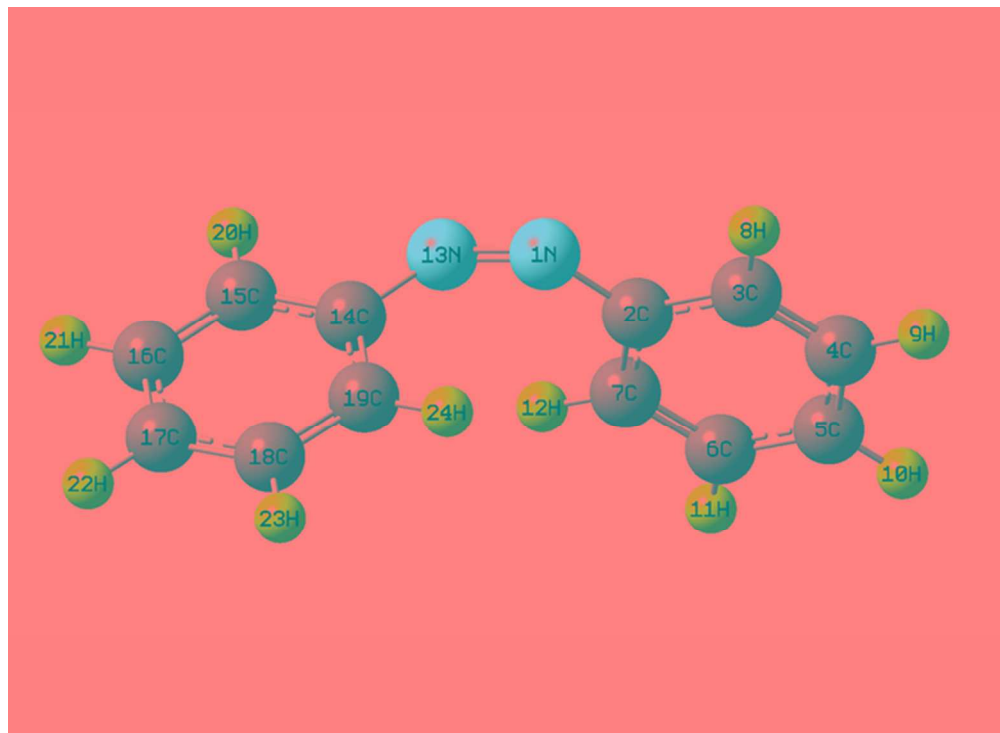
Fig. 1
62x45mm (300 x 300 DPI)
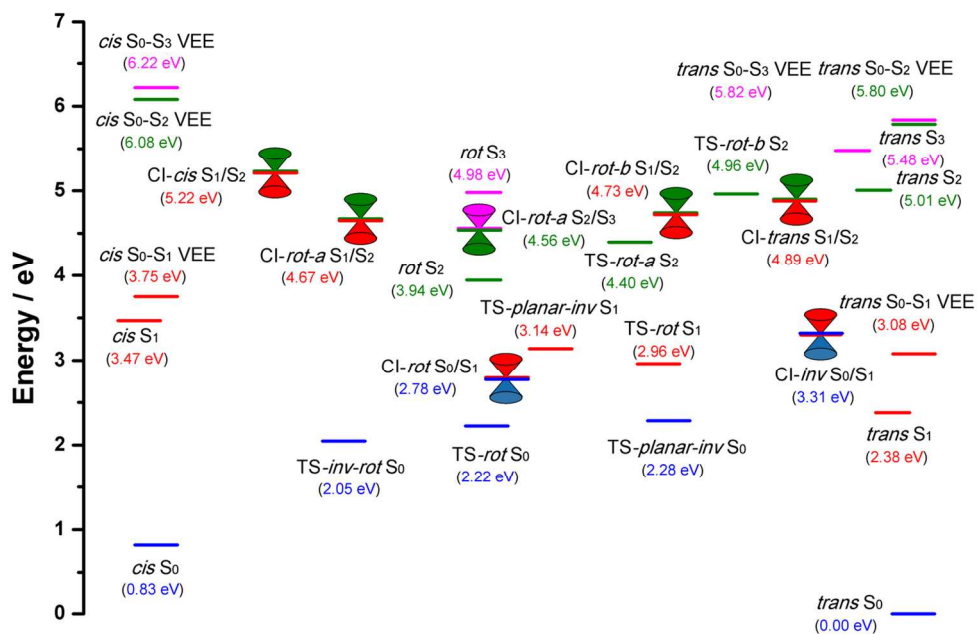
Fig. 2
125x93mm (300 x 300 DPI)
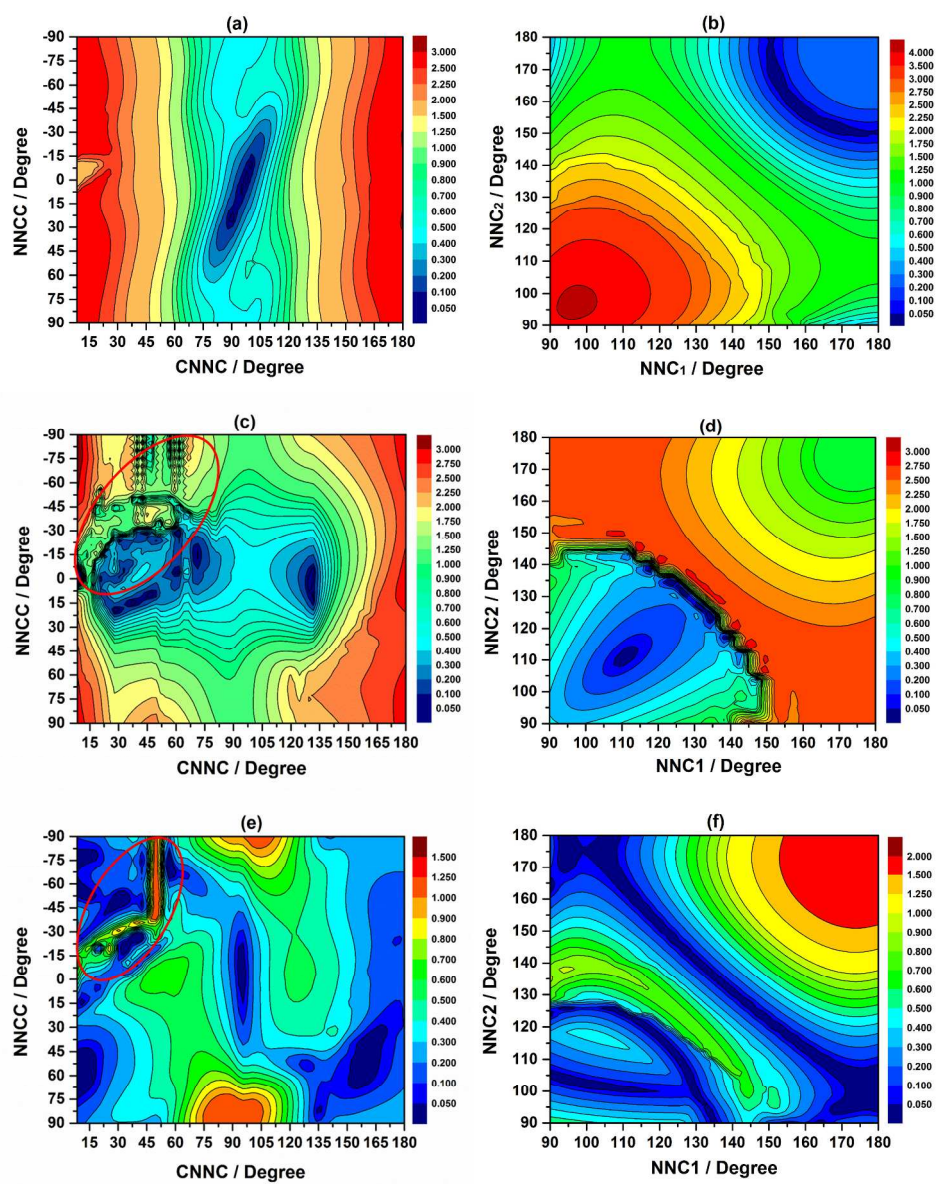
Fig. 3
215x274mm (300 x 300 DPI)

Scheme
186x203mm (300 x 300 DPI)
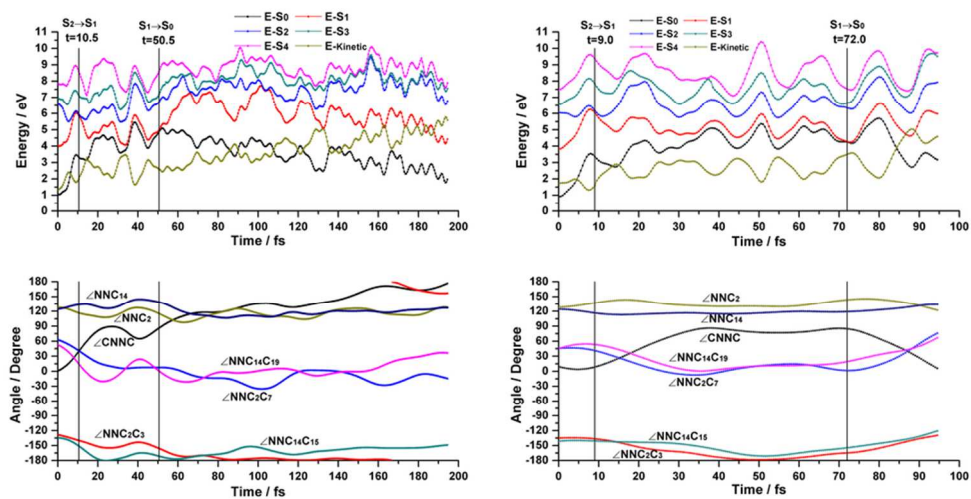
Fig. 4
84x42mm (300 x 300 DPI)
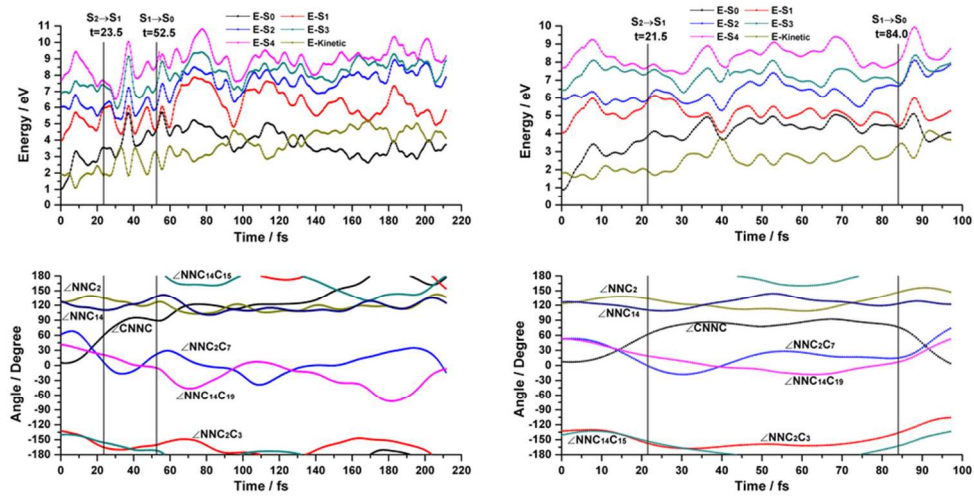
Fig. 5
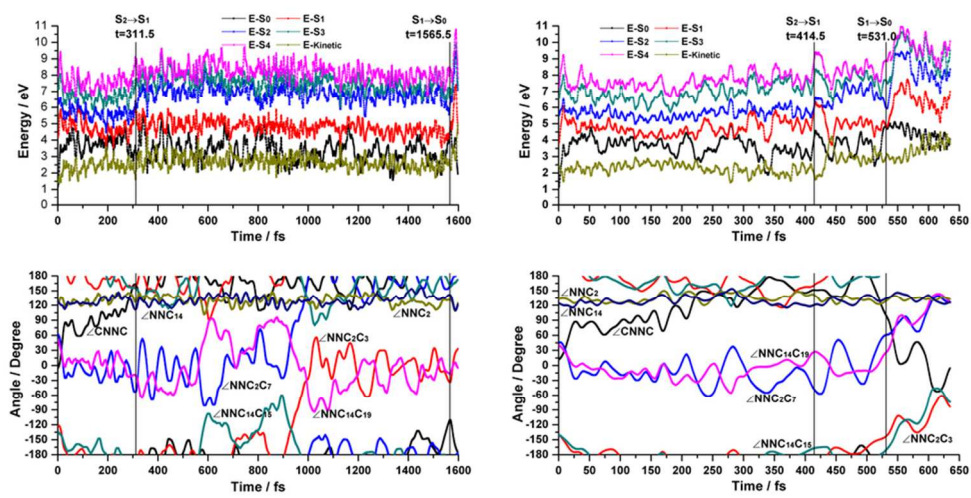84x42mm (300 x 300 DPI)
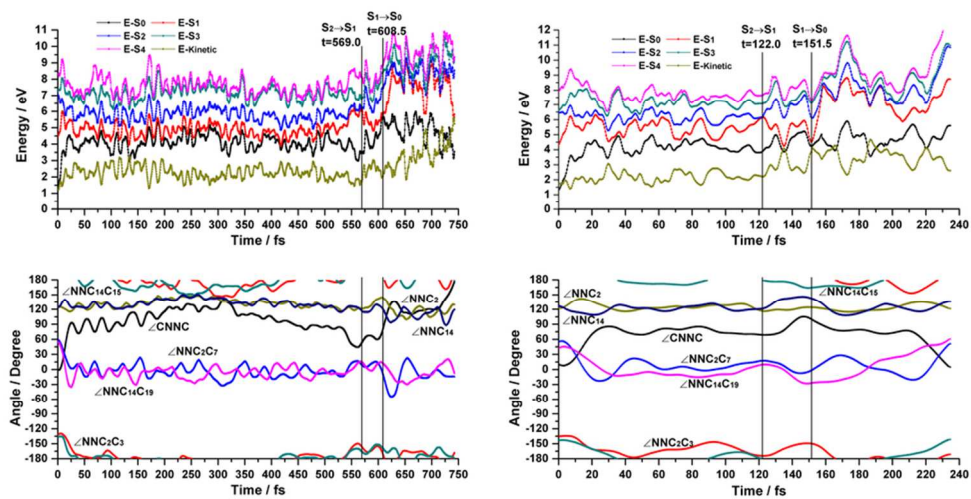
Fig. 6
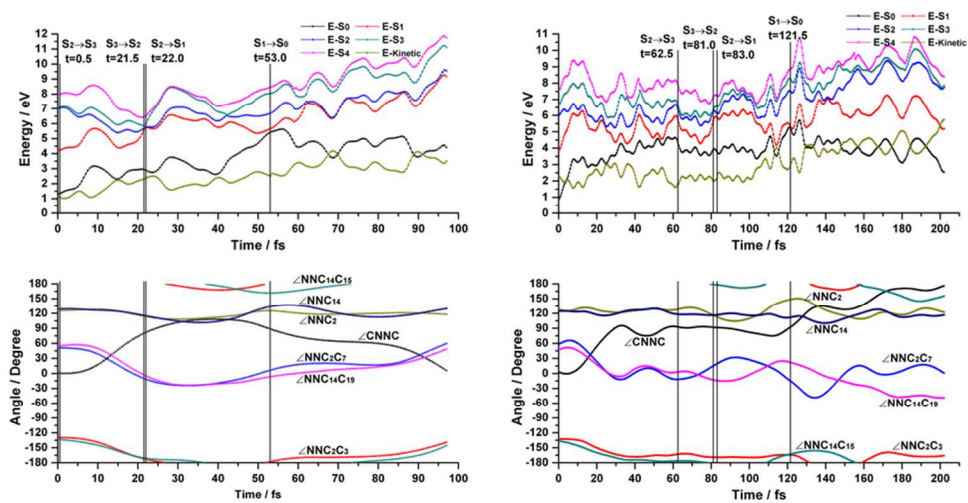84x42mm (300 x 300 DPI)

Fig. 7
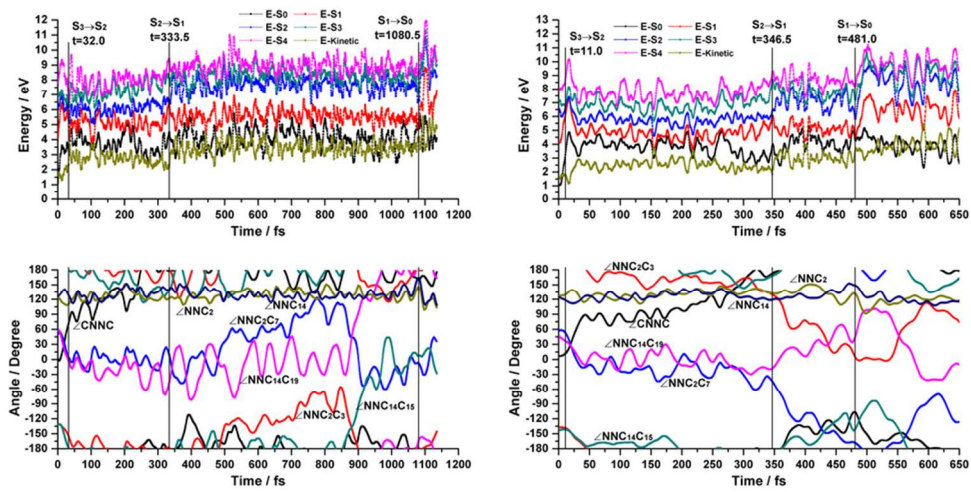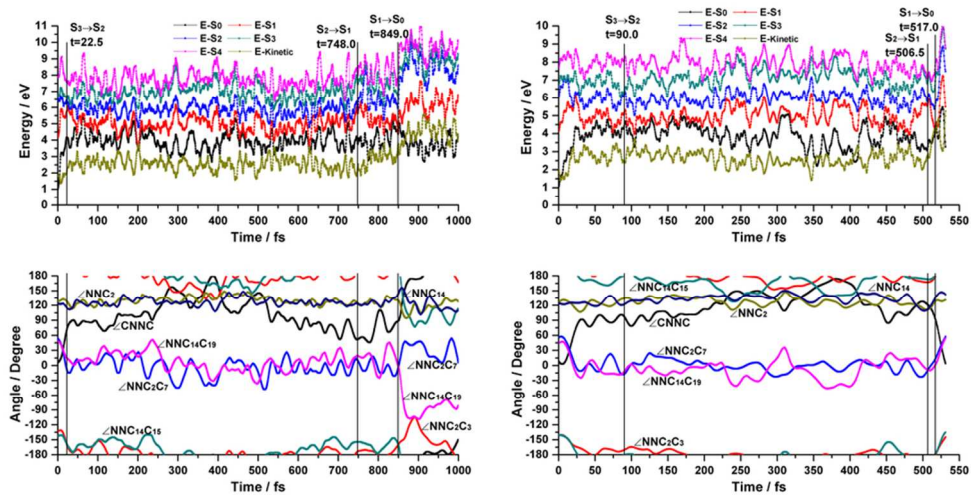84x42mm (300 x 300 DPI)

Fig. 8
84x42mm (300 x 300 DPI)

Fig. 9
84x42mm (300 x 300 DPI)

Fig. 10
84x42mm (300 x 300 DPI)